Hindawi Publishing Corporation
Journal of Nanoparticles
Volume 2014, Article ID 893459, 15 pages
http://dx.doi.org/10.1155/2014/893459

Research Article

Plasmonic and Thermooptical Properties of Spherical Metallic Nanoparticles for Their Thermoplasmonic and Photonic Applications

Victor K. Pustovalov,[1] Liudmila G. Astafyeva,[2] and Wolfgang Fritzsche[3]

[1] *Belarusian National Technical University, Nezavisimosti Prospect 65, 220013 Minsk, Belarus*
[2] *B.I. Stepanov Institute of Physics, National Academy of Sciences of Belarus, Nezavisimosti Prospect 68, 220072 Minsk, Belarus*
[3] *Leibniz Institute of Photonic Technology, 07702 Jena, Germany*

Correspondence should be addressed to Victor K. Pustovalov; pustovalovv@mail.ru
and Wolfgang Fritzsche; fritzsche@ipht-jena.de

Received 15 July 2014; Accepted 3 August 2014; Published 14 October 2014

Academic Editor: Amir Kajbafvala

Investigations and use of nanoparticles (NPs) as photothermal (PT) agents in laser and optical nanotechnology are fast growing areas of research and applications. The potential benefits of NPs applications include possibility for thermal imaging and treatment of materials containing of NPs, applications of NPs for light-to-thermal energy conversion, in catalysis, laser nanomedicine, and chemistry. Efficie y of applications of metallic NPs for laser and optical nanotechnology depends on plasmonic and thermophysical properties of NPs, characteristics of radiation, and surrounding medium. Here we present the results of comparative analysis of NP properties (plasmonic, thermooptical, and others) allowing selecting their parameters for thermoplasmonic and photonic applications. Plasmonic and thermooptical properties of several metallic (aurum, silver, platinum, cobalt, zinc, nickel, titanium, cuprum, aluminum, molybdenum, vanadium, and palladium) NPs are theoretically investigated and analysis of them is carried out. Investigation of the influence of NPs parameters (type of metal, radii, optical indexes, density, and heat capacity of NP material), characteristics of radiation (wavelength and pulse duration), and ambient parameters on plasmonic and thermophysical properties of NPs has been carried out. It was established that maximum value of thermooptical parameter (maximum NP temperature) can be achieved with the use of absorption efficie y factor of NP smaller than its maximum value.

1. Introduction

Recent advances in photothermal nanotechnology based on the use of nanoparticles (NPs) and optical (laser) radiation have been demonstrated for their great potential. In recent years, the laser-NP interaction, absorption, and scattering of radiation energy by NP have become of great interest and an increasingly important for topic in photonic and laser nanotechnology [1–27] (also see the references in these papers). The e are many reasons for this interest including application of NPs in different fields such as catalysis [1, 2], laser nanobiomedicine [3–11], nanooptics and nanoelectronics [12–15], laser processing of metallic NPs in nanotechnology [16–23], and light-to-heat conversion [24–27].

Most of these technologies rely on the position and strength of the surface plasmon on a nanosphere and the fact that NP will absorb and scatter radiation energy well at resonance wavelength. Successful applications of NPs in photonics and thermoplasmonics are based on appropriate plasmonic and optical properties of NPs. High absorption of radiation by NPs can be used for conversion of absorbed energy into NP thermal energy, heating of NP itself and ambient medium, and following photothermal phenomena in laser and optical nanotechnology and nanomedicine. High scattering of radiation is essential for optical diagnostics and imaging applications based on light scattering.

Metallic NPs are mostly interesting for different nanotechnologies among other NPs. First investigations of optical

properties of metallic NPs were carried out in [28, 29]. Th attempts to search for the "ideal" plasmonic NPs were carried out in many papers. Optical absorption efficie y of some metallic NPs was investigated in [28–33]. The mooptical analysis and selection of the properties of gold NPs for laser applications in nanotechnology were carried out in [8, 26, 34]. Searching for better plasmonic materials (metals) was carried out in [13, 32, 35, 36] based on investigations of quality factors of each metal. Different metallic NPs (gold, silver, platinum, zinc, etc.) were used in [1–36]. Gold and silver NPs were considered as the most appropriate ones and widely used in experiments. Methods of chemical synthesis of metallic NPs have been developed and presented in [37–39].

On the other side, a comparative analysis of optimal parameters of different metallic NPs for using them as PT agents in thermoplasmonics and laser nanotechnology is still missing. Here we propose the results for analysis of the NP properties for their photonic and thermoplasmonic applications.

Plasmonic and thermooptical properties of metallic NPs were theoretically investigated and compared in this paper based on computer modeling. We carry out complex investigation of the plasmonic and thermooptical properties of spherical metallic NPs for their interaction with optical (laser) radiation placed (embedded) in some ambient medium. We investigated the influence of the parameters of radiation, NP, and ambient medium on the properties of this interaction.

2. Plasmonic and Thermooptical Parameters of Nanoparticles

Among different characteristics of NPs, laser radiation, and ambient medium that will determine NP plasmonic and thermooptical properties we can note the following ones:

(1) laser (optical) radiation—(a) pulse duration t_P, (b) wavelength λ, and (c) radiation (laser) exposure (energy density) E_0, intensity $I_0 = E_0/t_P$;

(2) spherical nanoparticle—(a) type of NP metal with its values of density ρ_0, heat capacity c_0, optical indexes of refraction $n_{0\lambda}$, and absorption $\chi_{0\lambda}$ of NP metal and (b) NP radius r_0;

(3) nonabsorbing surrounding medium—(a) coeffici t of thermal conductivity k_∞ = const and (b) optical indexes of refraction n_λ.

Consider the parameters that characterize the transformation of radiation energy in the processes of NP-radiation interaction.

Efficiency factors of absorption K_{abs}, scattering K_{sca}, and extinction K_{ext} of radiation by NP [29] determine the optical properties of NP.

Parameter P_1 describes the correlation between absorption and scattering of radiation by NP. Parameter P_1 characterizes the contribution of the processes of absorption and scattering to the general energy balance of the NP:

$$P_1 = \frac{K_{abs}}{K_{sca}}. \tag{1}$$

The efficiency factor of absorption of laser radiation by NPs K_{abs} can be greater or smaller than the factor of scattering of radiation by NP K_{sca} in the cases of predominant role of absorption or scattering in the process of radiation interaction with NP:

$$K_{abs} > K_{sca}, \qquad P_1 > 1, \tag{2a}$$

$$K_{abs} < K_{sca}, \qquad P_1 < 1. \tag{2b}$$

Th parameter $\Delta T_0/E_0$ [6–8] can be used for determination of thermooptical properties of NPs

$$\frac{\Delta T_0}{E_0} = \frac{K_{abs} r_0}{4 k_\infty t_P}\left[1 - \exp\left(-\frac{t_P}{\tau_0}\right)\right], \tag{3}$$

$\tau_0 = \rho_0 c_0 r_0^2/3k_\infty$—characteristic time for heating and cooling of NP. Thi parameter determines the increase of NP temperature $\Delta T_0 = T_{max} - T_\infty$ under action of radiation energy density with value $E_0 = 1\,\mathrm{J/cm^2}$, T_{max}, maximum temperature of NP at $t = t_P$, and T_∞, initial NP temperature.

Parameter $\Delta T_0/E_0$ (3) may be viewed as NP heating efficie y under action of radiation energy with energy density E_0. For $t_P < \tau_0$ and $t_P > \tau_0$ the parameter $\Delta T_0/E_0$ will be approximately determined by the following (see (3)):

$$t_P < \tau_0, \quad \frac{\Delta T_0}{E_0} \approx \frac{3K_{abs}}{4\rho_0 c_0 r_0}, \tag{4a}$$

$$t_P > \tau_0, \quad \frac{\Delta T_0}{E_0} \approx \frac{K_{abs} r_0}{4 k_\infty t_P}. \tag{4b}$$

In general, the parameter $\Delta T_0/E_0$ ((3), (4a), and (4b)) depends on characteristics of radiation, λ and t_P, metallic NP, $K_{abs}(\lambda)$, r_0, c_0, and ρ_0, and ambient medium, k_∞, index of medium refraction n_λ. Combinations $K_{abs}(r_0)/r_0$ and $K_{abs}(r_0)r_0$ in (4a) and (4b) determine the range of radii r_0 appropriate for the achievement of the maximum value of T_0 under a fi ed value of λ, $K_{abs}(\lambda)$. The combination $1/c_0\rho_0$ determines the influence of NP metal properties on the maximum value of T_0. Values of k_∞ and n_λ determine the influence of surrounding medium on thermooptical properties of NPs. Th parameter of $\Delta T_0/E_0$ does not depend on parameters of radiation (t_P) and ambience (k_∞) in (4a). Th selection of mentioned parameters in (3), (4a), and (4b) can provide maximum values ΔT_0 for concrete values of E_0.

We will investigate the influence of all characteristics of NPs, laser radiation, and ambient medium mentioned above on plasmonic and thermooptical properties of metallic NPs. Comparative analysis of the properties of metallic NPs and their efficie y for photonic applications in nanotechnology

have to use the following set of plasmonic and thermooptical parameters of the laser-NP interaction processes:

(i) efficie y factors of absorption K_{abs}, scattering K_{sca}, and extinction K_{ext} of radiation by spherical NP;

(ii) parameter of P_1 (1);

(iii) parameter $\Delta T_0/E_0$ ((3), (4a), and (4b)).

3. Plasmonic and Thermooptical Properties of NPs

Calculations and analysis of plasmonic and thermooptical properties of NPs have been carried out in our investigations. We numerically calculated efficiency factors of absorption K_{abs}, scattering K_{sca}, and extinction K_{ext} of radiation with wavelength λ by spherical homogeneous metallic NP based on generalized Mie theory [29]. Values of optical indexes of refraction and absorption of metals and surrounding media were used from [40–42]. After that, we use (1) and (3) for calculation of the parameters P_1 and $\Delta T_0/E_0$. All figu es presented describe the dependences of efficie y factors of absorption K_{abs}, scattering K_{sca}, and extinction K_{ext}, parameters P_1 and $\Delta T_0/E_0$ for metallic NPs on wavelength of radiation, NP radii, pulse duration t_P, and characteristics of surrounding media. Simultaneous comparative investigation of the dependences of K_{abs}, K_{sca}, K_{ext}, and $\Delta T_0/E_0$ on λ, r_0, and other characteristics is very complex and hard task. We have divided this task into two steps. A first step is the calculation and investigation of the dependences of K_{abs}, K_{sca}, K_{ext}, P_1, and $\Delta T_0/E_0$ on λ for some fixed values of r_0, t_P, and selected NP metal and surrounding medium. Second one is the investigation of the dependences of K_{abs}, K_{sca}, K_{ext}, P_1, and $\Delta T_0/E_0$ on r_0 for some fixed values of λ, t_P, and selected NP metal and surrounding medium. Thi allows investigating complex task step by step and present clear dependences of K_{abs}, K_{sca}, K_{ext}, P_1, and $\Delta T_0/E_0$ on one parameter when other parameters are constant. Figures 1–7 present the dependences of K_{abs}, K_{sca}, K_{ext}, P_1, and $\Delta T_0/E_0$ on λ, r_0, t_P, and optical indexes of metals and surrounding media.

Th heat fl w from NP, placed in liquids, amorphous solids, and so forth, can be well described by the diffusive heat equation, when mean free path of heat transporter (molecule, etc.) is very short, like $\sim 10^{-8}$ cm in mentioned media [43, 44], and this one is much smaller than characteristic NP radii of r_0 ~10–100 nm. In gases at atmospheric pressure the mean free path of molecules is about $\sim 10^{-5}$ cm and diff sive heat equation can be applied to the heat exchange of NP with gaseous medium for $r_0 \geq 100$ nm. Methods of kinetic equation or molecular dynamics should be used for the description of heat exchange of NP in this case. But during ultrashort laser pulse action with $t_P \sim 10^{-10}$–10^{-12} s on NP we can neglect NP heat exchange with surrounding gas during laser action and calculate parameter $\Delta T_0/E_0$ for $t_P = 1 \times 10^{-12}$ s using (4a). Th dependence $\Delta T_0/E_0(\lambda)$ for $t_P \sim 1 \times 10^{-10}$ s practically coincides with this one for $t_P = 1 \cdot 10^{-12}$ s and only one dependence $\Delta T_0/E_0(\lambda)$ is presented in Figures 1–6 for ambient air and $t_P = 1 \cdot 10^{-12}$ s. We can note that the values of $\Delta T_0/E_0$ for $t_P \sim 10^{-12}$ s can be used as upper boundaries of NP heating ($\Delta T_0 = T_{max} - T_\infty$) without NP heat exchange.

Th positions of maximum values of efficie y factors of K_{abs}^{max}, K_{sca}^{max}, and K_{ext}^{max} on λ axis are denoted in Figures 1–6 by different vertical lines and locations λ_{abs}^{max} of maximum value of absorption factor K_{abs}^{max} on axis λ are denoted by solid lines, K_{sca}^{max}, dashed lines, and λ_{sca}^{max}, K_{ext}^{max}, dashed-dotted lines, and λ_{ext}^{max} in the case of different values of λ_{abs}^{max}, λ_{sca}^{max}, and λ_{ext}^{max}. In the case of equal values of λ_{abs}^{max}, λ_{sca}^{max}, and λ_{ext}^{max} the location of coincident values of K_{abs}^{max}, K_{sca}^{max}, and K_{ext}^{max} is denoted by solid lines. In some cases additional solid lines denote the locations of the formation of new maximums of efficie y factors (see Figures 3(c), 3(g)) or the points of sharp bend of the dependence of K_{abs} on λ (see Figures 4(i) and 4(j)). Horizontal dashed lines in Figures 1(d), 1(h), 1(l)–6(d), 6(h), and 6(l) denote the value of $P_1 = 1$.

Figures 1–3 present the dependences of efficie y factors of K_{abs}, K_{sca}, and K_{ext} of radiation, parameters $\Delta T_0/E_0$ for $t_P = 1 \cdot 10^{-8}$, $1 \cdot 10^{-12}$ s, and P_1 for homogeneous metallic Au (Figure 1), Ag (Figure 2), and Pt (Figure 3) NPs with radii $r_0 = 10$, 25, and 50 nm on wavelengths λ. NPs are placed in silica, water, and air ambient nonabsorbing media. Optical constants (indexes of refraction n_λ and absorption λ) are changed in the ranges for silica $n_\lambda \approx 1.51 - 1.45$, water $n_\lambda \approx 1.39 - 1.33$, air $n_\lambda \approx 1.0$, and $\varkappa_\lambda \approx 0$ for all ambiences with increasing wavelength λ in the spectral interval ~200–1000 nm.

Th dependences of efficie y factors of K_{abs}, K_{sca}, and K_{ext} on λ for fixed values of r_0 have complicated forms. Values of K_{abs}^{max} are placed at $\lambda_{abs}^{max} \sim 510$–530 nm for Au NPs and $\lambda_{abs}^{max} \sim 380$–410 nm for Ag NPs for $r_0 = 10$, 25, and 50 nm and different ambiences. Consequently the absorption of radiation is determined by plasmon resonances of silver and gold NPs in the fiel of electromagnetic (laser) radiation. Values of K_{abs} are decreased in UV and NIR spectral intervals out of plasmon wavelengths and especially for Ag NPs these values undergo sharp decrease up to 10^2-10^3 times. We can note a slight decrease of K_{abs} for Au NP in the UV spectral interval in comparison with NIR spectral interval. The behavior of dependences of K_{sca} on wavelength λ is analogous for the dependence of $K_{abs}(\lambda)$. Maximum value of K_{sca}^{max} for Ag NPs achieves $K_{sca} \sim 11 \div 15$ in the interval of $\lambda \sim 410 \div 430$ nm and $r_0 = 25$ nm. Dependence of K_{ext} on λ presents itself the sum of the dependences of $K_{abs}(\lambda)$ and $K_{sca}(\lambda)$. The values of K_{abs}^{max} and K_{ext}^{max} for Au, Pt NPs for $r_0 = 10$ and 25 nm and for Ag NPs $r_0 = 10$ nm practically coincide with each other and for different ambiences (see Figures 1–3). But for $r_0 = 50$ nm values of K_{sca}^{max} and K_{ext}^{max} are greater than K_{abs}^{max}. This fact was also noted in [31]. An increase of r_0 may lead to increase or decrease of the maximum values of K_{abs}, K_{sca}, and K_{ext}. Coincidence of different vertical lines in figu es means the coincidence of corresponding values of optical parameters. Placements of K_{ext} at $\lambda \sim 292$ nm and 443 nm for NPs in water for $r_0 = 25$ and 50 nm quantitatively coincide with experimental data [45].

Placements of maximum values of K_{abs}, K_{sca}, and K_{ext} on axis λ can be different in some cases (Figures 1(c), 1(g), 1(k)–3(c), 3(g), and 3(k)). Th formation of additional maximums

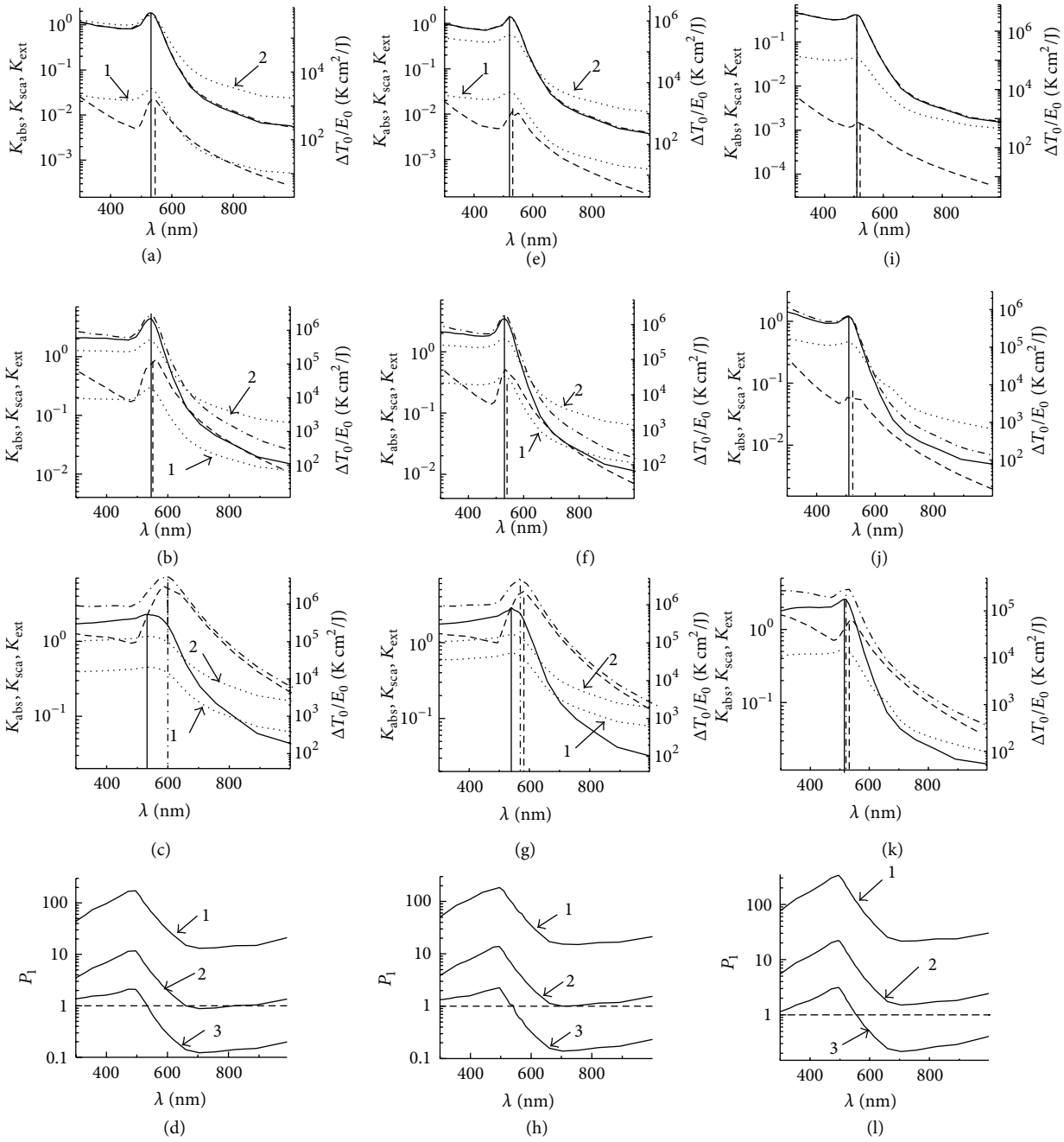

Figur e 1: Dependences of efficie y factors of absorption K_{abs} (solid), scattering K_{sca} (dashed), and extinction K_{ext} (dashed-dotted) of radiation and parameter $\Delta T_0/E_0$ (dotted) for $t_P = 1 \cdot 10^{-8}$ (1), $1 \cdot 10^{-12}$ (2) s for **Au** NPs with radii $r_0 = 10$ ((a), (e), and (i)), 25 ((b), (f), and (j)), and 50 ((c), (g), and (k)) nm, and the dependences of parameter P_1 ((d), (h), and (l)) for Au NPs with radii $r_0 = 10$ nm (1), $r_0 = 25$ nm (2), and $r_0 = 50$ nm (3) on wavelengths λ. Au NPs are placed in silica ((a)–(d)), water ((e)–(h)), and air ((i)–(l)).

of K_{abs}, K_{sca}, and K_{ext} on axis λ can be connected with possible manifestation of resonances with higher orders (Figures 3(c) and 3(g) Pt NPs). An increase of NP radii to $r_0 = 50$ nm shift the maximum values of K_{sca} and K_{ext} in the region of greater values of λ. The value of shift of $\Delta\lambda_{max} = \lambda_{max}(K_{abs}) - \lambda_{max}(K_{sca})$ increases with increasing of r_0, for $r_0 = 10$ nm $\Delta\lambda_{max} \sim 5$–13nm for all surroundings, and for $r_0 = 50$ nm this one achieves values of $\Delta\lambda_{max} \sim 15$–70 nm. The e values increase with increasing of n_λ from air to silica for Au, Ag, Pt NPs. But K_{sca}^{max} and K_{ext}^{max} have been shifted compared to the position of $K_{abs}^{max}(\lambda_{abs}^{max})$ up to 80–120 nm (Figures 1(c), 2(c), and 2(g)) to bigger values of λ with increasing of r_0.

Figure 3 shows for **Pt** NPs that maximums of absorption K_{abs}^{max} and scattering K_{sca}^{max} for $r_0 = 10$ nm are accordingly situated at wavelengths $\lambda_{abs}^{max} = 248$ nm and $\lambda_{sca}^{max} = 150$ nm in silica. Increase of r_0 leads to shifting of K_{abs}^{max}, K_{sca}^{max}, and

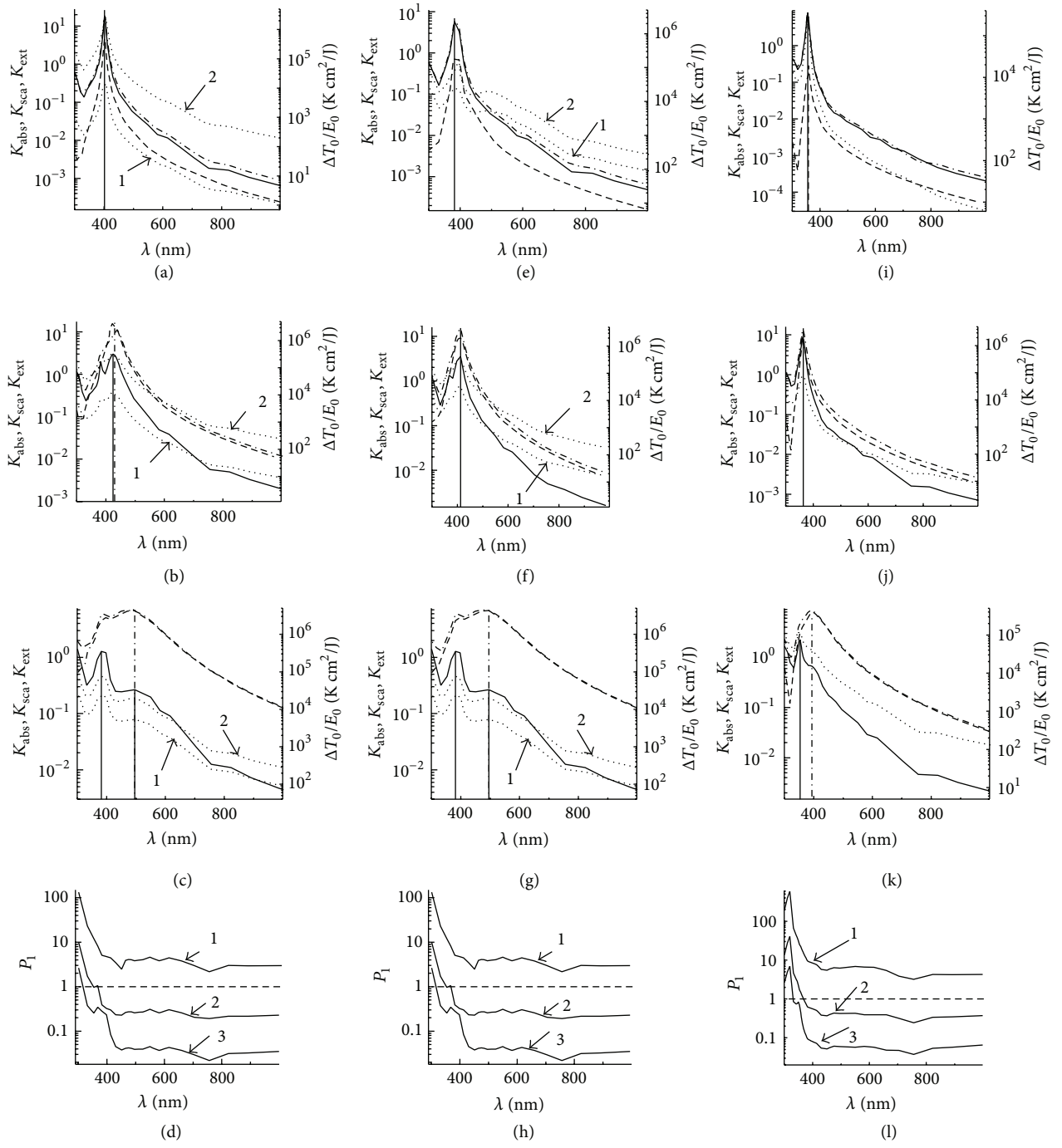

Figur e 2: Dependences of K_{abs} (solid), K_{sca} (dashed), and K_{ext} (dashed-dotted) of radiation and parameter $\Delta T_0/E_0$ (dotted) for $t_P = 1 \cdot 10^{-8}$ (1), $1 \cdot 10^{-12}$ (2) s for **Ag** NPs with radii $r_0 = 10$ ((a), (e), and (i)), 25 ((b), (f), and (j)), and 50 ((c), (g), and (k)) nm, and the dependences of parameter P_1 ((d), (h), and (l)) for Ag NPs with radii $r_0 = 10$ nm (1), $r_0 = 25$ nm (2), and $r_0 = 50$ nm (3) on wavelengths λ. Ag NPs are placed in silica ((a)–(d)), water ((e)–(h)), and air ((i)–(l)).

K_{ext}^{max} to bigger values of λ; for example, K_{abs}^{max} is shift d from $\lambda_{abs}^{max} \sim 220$–$250$ nm for $r_0 = 10$ nm to $\lambda_{abs}^{max} \sim 450$–$480$ nm for $r_0 = 50$ nm in silica and water. But for air this shift is from $\lambda_{abs}^{max} \sim 220$ nm for $r_0 = 10$ nm to $\lambda_{abs}^{max} \sim 310$ nm for $r_0 = 50$ nm. Maximum values of K_{abs}^{max}, K_{sca}^{max}, and K_{ext}^{max} are at the values of λ_{abs}^{max}, λ_{sca}^{max}, and λ_{ext}^{max} for $r_0 = 50$ nm. Moreover two maximum values of K_{abs}^{max} are formed for $r_0 = 50$ nm in silica at $\lambda_{abs}^{max} = 317.9$ and 495.9 nm and in water at $\lambda_{abs}^{max} = 290$ and 477 nm.

For Au NPs, dependences of P_1 on λ are determined by the dependences of K_{abs} and K_{sca} on λ. Increase of r_0 from $r_0 = 10$ nm to $r_0 = 50$ nm leads to a decrease of the parameter P_1 from the values of about $P_1 \sim 20$–300 for $\lambda \sim 300$–1000 nm up to values of about $P_1 \sim 0.1$–0.3 for $\lambda \sim 600$–1000 nm.

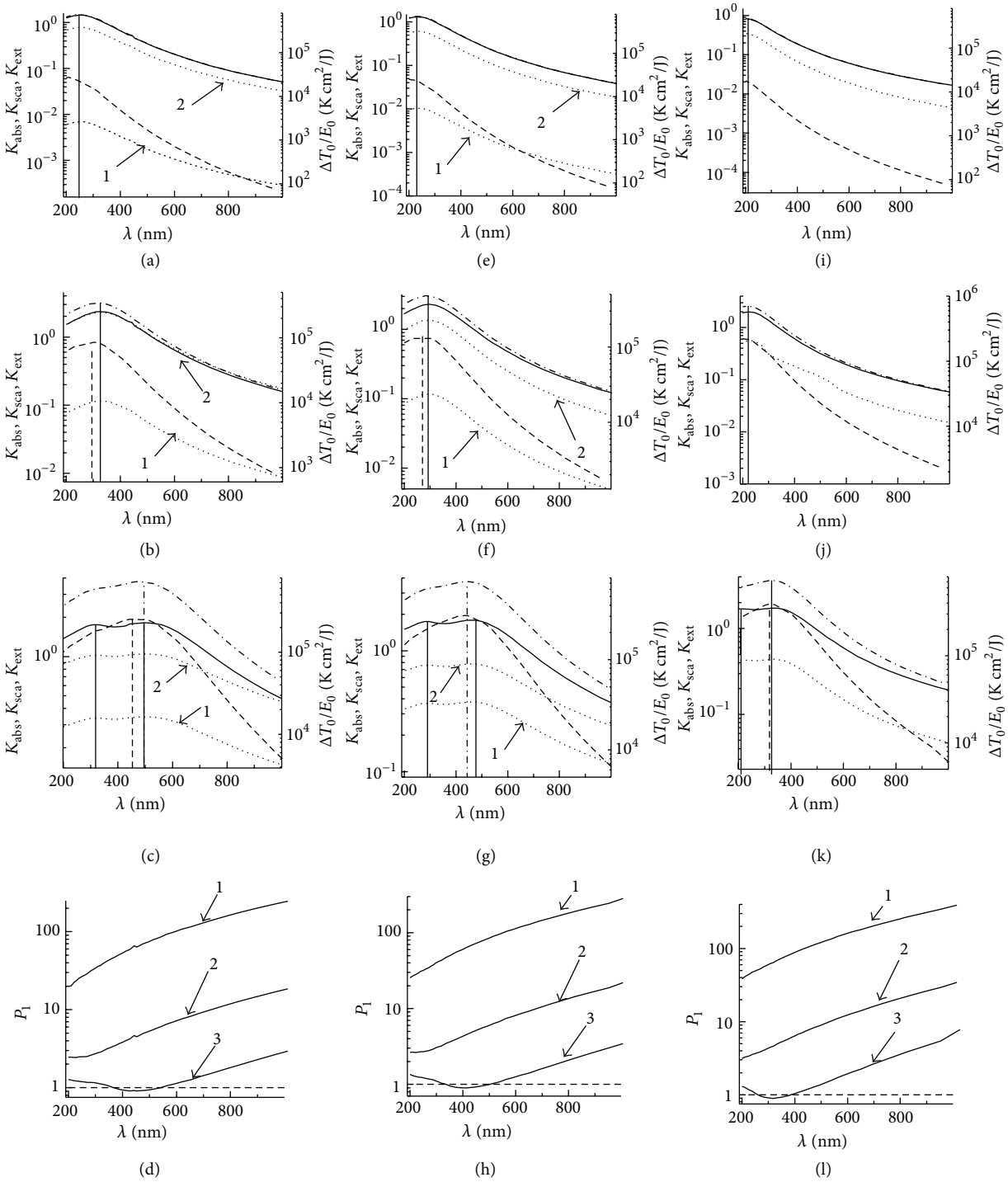

Figur e 3: Dependences of K_{abs} (solid), K_{sca} (dashed), and K_{ext} (dashed-dotted) of radiation and parameter $\Delta T_0/E_0$ (dotted) for $t_P = 1 \cdot 10^{-8}$ (1), $1 \cdot 10^{-12}$ (2) s for **Pt** NPs with radii $r_0 = 10$ ((a), (e), and (i)), 25 ((b), (f), and (j)), and 50 ((c), (g), and (k)) nm, and the dependences of parameter P_1 ((d), (h), and (l)) for **Pt** NPs with radii $r_0 = 10$ nm (1), $r_0 = 25$ nm (2), and $r_0 = 50$ nm (3) on wavelengths λ. Pt NPs are placed in silica ((a)–(d)), water ((e)–(h)), and air ((i)–(l)).

It means sharp increase of radiation scattering by NPs with an increase of NP r_0. For Ag NPs, a sharp decrease with increasing of λ in the spectral interval $\lambda \sim 300$–400 nm is observed and is approximately constant in the interval $\lambda \sim 300$–1000 nm. General feature for all presented dependences of $P_1(\lambda, r_0)$ is the decrease of P_1 with increasing of r_0 for the whole spectral interval $\lambda \sim 200$–1000 nm.

Th dependences of P_1 on λ for Pt NPs increase with increasing λ for $r_0 = 10$ and 25 nm and achieve values of $P_1 \sim 3$–200 for the whole spectral interval because of

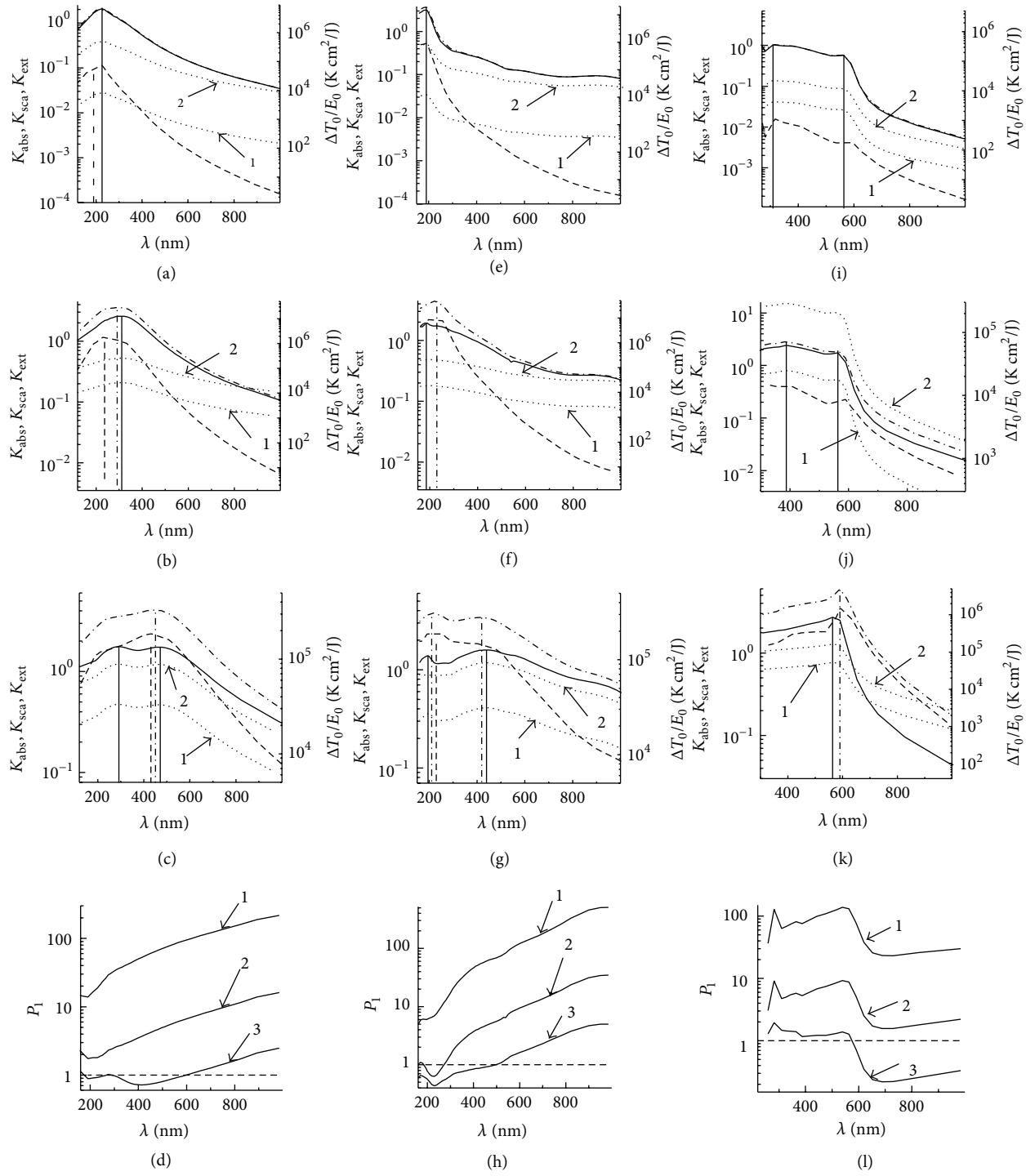

Figure 4: Dependences of factors K_{abs} (solid), K_{sca} (dashed), and K_{ext} (dashed-dotted) of radiation for homogeneous metallic **Pd** ((a), (b), (c), and (d)), **Cu** ((e), (f), (g), and (h)), and **Mo** ((i), (j), (k), and (l)) NPs, placed in water, with radii $r_0 = 10$ ((a), (d), and (g)), 25 ((b), (e), and (h)), and 50 ((c), (f), and (i)) nm, parameter $\Delta T_0/E_0$ (dotted) for $t_P = 1 \cdot 10^{-8}$ (1), $1 \cdot 10^{-12}$ (2) s, and dependences of parameter P_1 ((d), (h), and (l)) for 10 (1), 25 (2), and 50 (3) nm on wavelengths λ.

sharp decreasing of K_{sca} with increase of λ (see Figure 3). Th parameter P_1 is smaller than 1, $P_1 < 1$, for $r_0 = 50$ nm and the narrow wavelength interval ~350–500 nm for diff rent surroundings.

Figures 1–3 describe the influence of the medium refraction indexes and thermal properties on plasmonic and thermooptical properties of Au, Ag, and Pt NPs. Concrete values of K_{abs}^{max} and k_∞ determine the influence of different

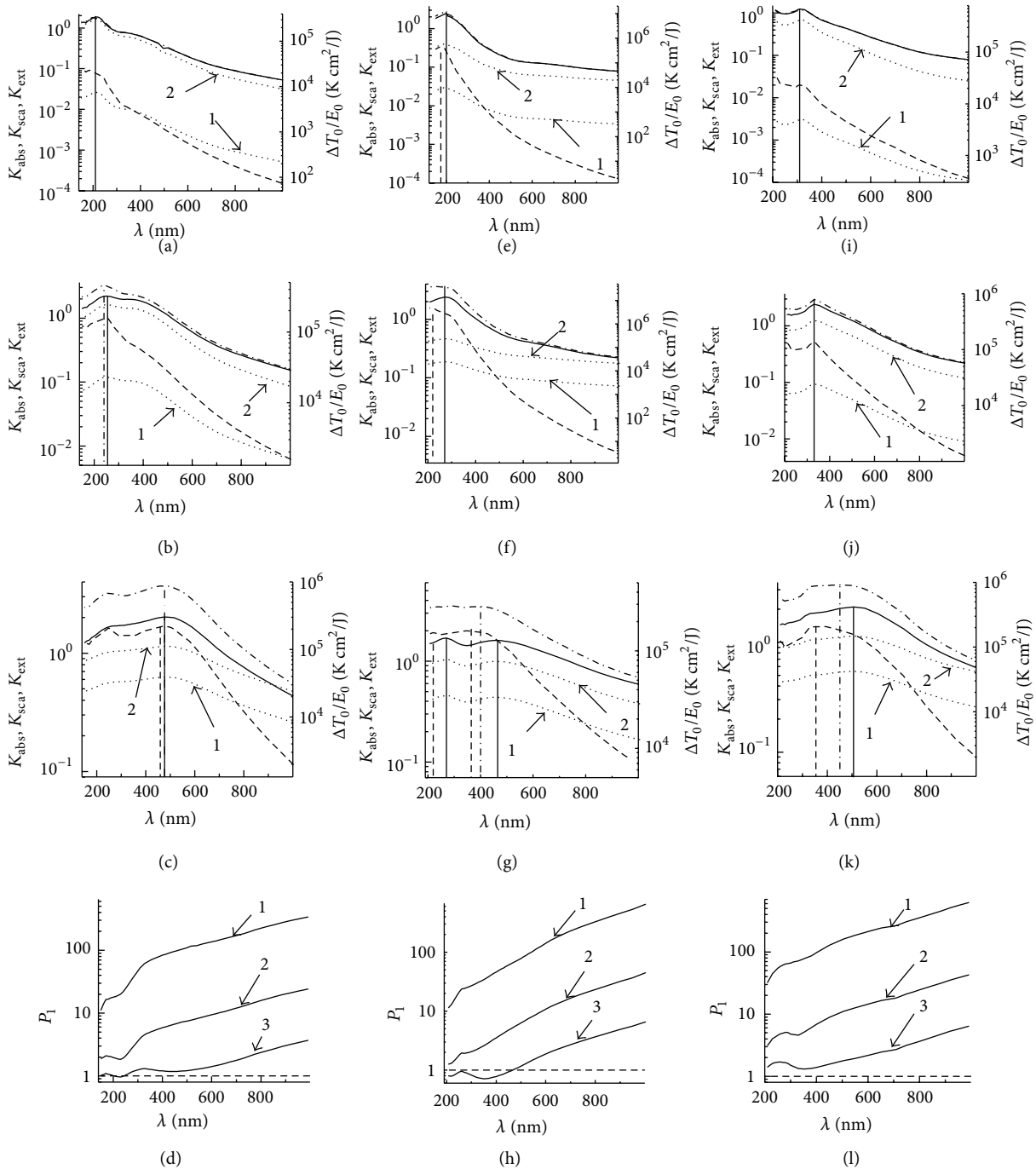

Figure 5: Dependences of factors K_{abs} (solid), K_{sca} (dashed), and K_{ext} (dashed-dotted) of radiation for homogeneous metallic **Ni** ((a), (b), (c), and (d)), **V** ((e), (f), (g), and (h)), and **Ti** ((i), (j), (k), and (l)) NPs, placed in water, with radii r_0 = 10 ((a), (d), and (g)), 25 ((b), (e), and (h)), and 50 ((c), (f), and (i)) nm, parameter $\Delta T_0/E_0$ (dotted) for $t_P = 1 \cdot 10^{-8}$ (1), $1 \cdot 10^{-12}$ (2) s, and dependences of parameter P_1 ((d), (h), and (l)) for 10 (1), 25 (2), and 50 (3) nm on wavelengths λ.

surroundings on the value of $\Delta T_0/E_0$ for different t_P (see (3)). Th wavelength shift $\Delta\lambda_{max}$ exists between maximums of K_{abs}^{max} from one side and maximums of K_{sca}^{max} and K_{ext}^{max} from a second side for silica and water. Maximum values and dependences of K_{abs}, K_{sca}, and K_{ext} on wavelength are qualitatively close to each other for r_0 = 10, 25, and 50 nm.

The decrease of refraction index from n_λ = 1.51 for silica to n_λ = 1.00 for air leads to shifting of λ_{max} for all efficie y factors for K_{abs} from ~545 nm to ~510nm and for K_{sca} and K_{ext} from 600 nm to 510 nm. Decrease of n_λ for silica to n_λ = 1.00 (air) leads to decrease of values of K_{abs}, K_{sca}, and K_{ext} up to 4 times for r_0 = 10 and 25 nm, but for r_0 = 50 nm

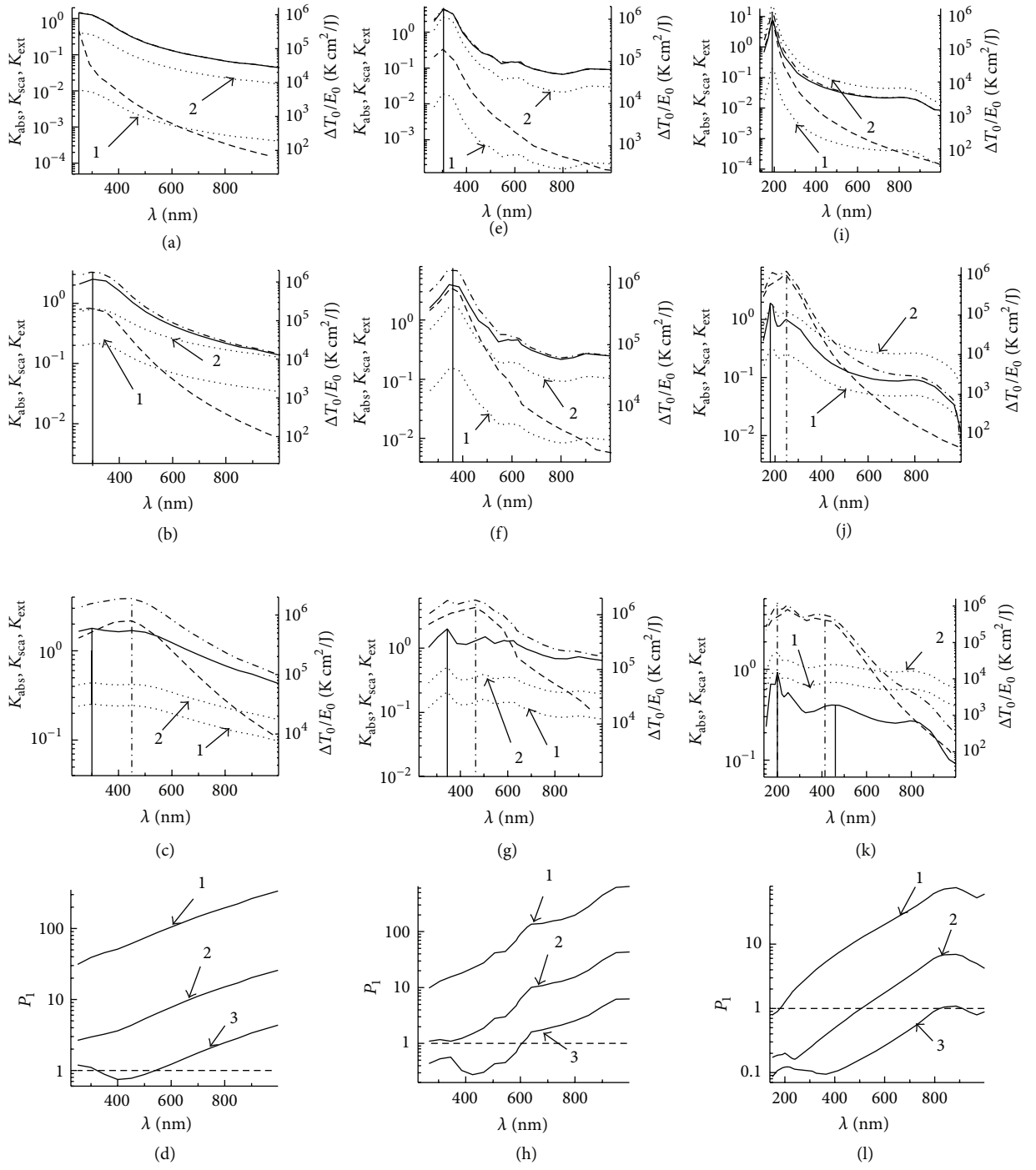

Figure 6: Dependences of factors K_{abs} (solid), K_{sca} (dashed), and K_{ext} (dashed-dotted) of radiation for homogeneous metallic **Co** ((a), (b), (c), and (d)), **Zn** ((e), (f), (g), and (h)), and **Al** ((i), (j), (k), and (l)) NPs, placed in water, with radii $r_0 = 10$ ((a), (d), and (g)), 25 ((b), (e), and (h)), and 50 ((c), (f), and (i)) nm, parameter $\Delta T_0/E_0$ (dotted) for $t_P = 1 \cdot 10^{-8}$ (1), $1 \cdot 10^{-12}$ (2) s, and dependences of parameter P_1 ((d), (h), and (l)) for 10 (1), 25 (2), and 50 (3) nm on wavelengths λ.

the dependence of maximum values of K_{abs}, K_{sca}, and K_{ext} is rather weak and leads to the smoothing of plasmonic peaks of the dependences of $K(\lambda)$, first of all, for $r_0 = 10, 25$ nm.

Th spectral dependence of $\Delta T_0/E_0(\lambda)$ is determined by the dependence of $K_{abs}(\lambda)$ for all values of r_0, because of dependence $\Delta T_0/E_0 \sim K_{abs}(\lambda)$ in (3), (4a), and (4b). Th influence of NP radius r_0 is directly realized on the value of $\Delta T_0/E_0$ and it is determined by the dependence of $K_{abs}(r_0)$ and value of r_0 in (3), (4a), and (4b). Parameters of surroundings influence the value of $\Delta T_0/E_0$ by the value of $K_{abs}(n_\lambda)$.

Th values of $\Delta T_0/E_0$ for $t_P = 1 \times 10^{-8}$ s are, as a rule, smaller in comparison with other ones for $t_P = 1 \times 10^{-12}$ s. It is determined by the influence of heat exchange of NP with

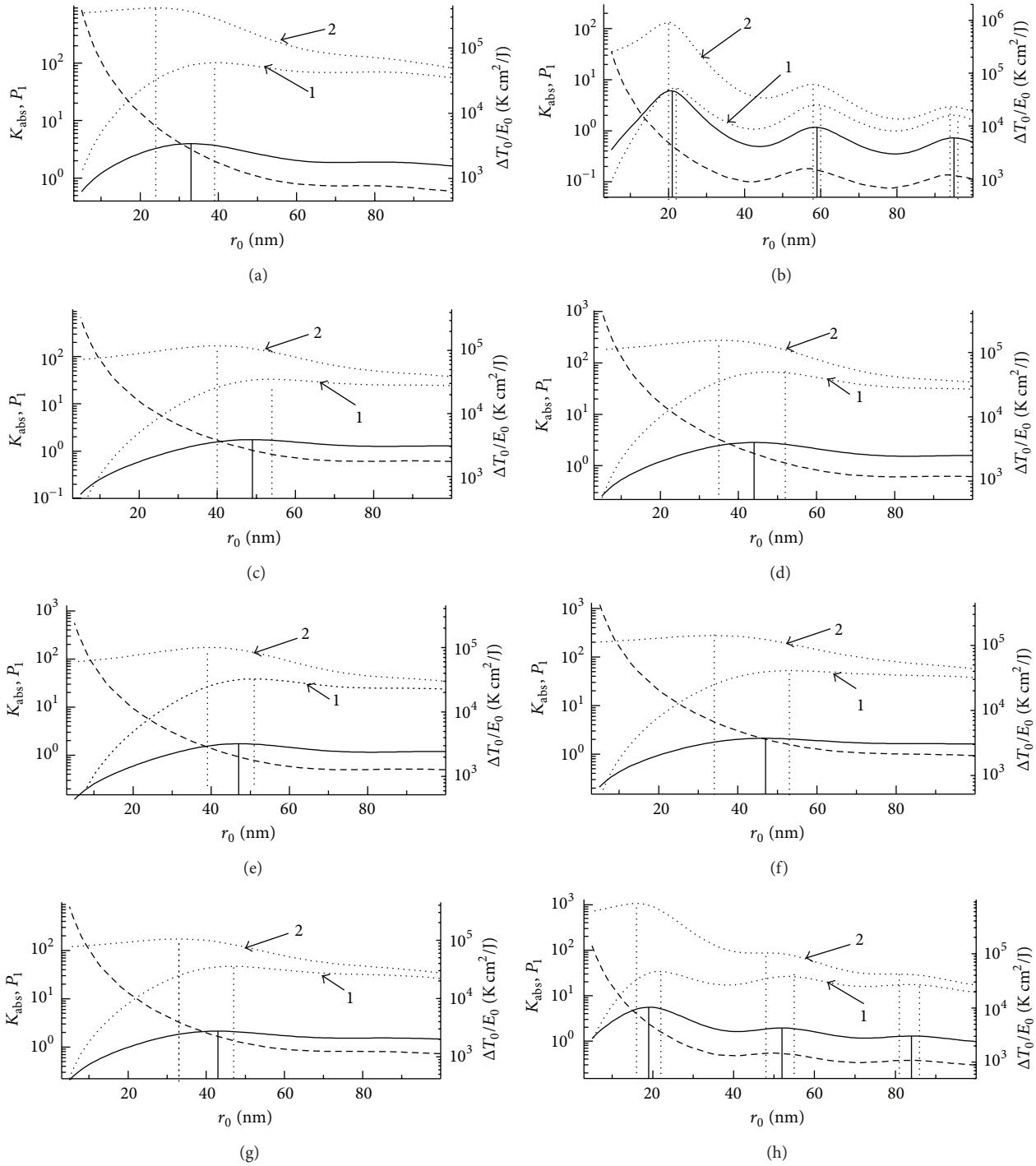

Figur e 7: Dependences of K_{abs} (solid lines refer to the left axis), parameter P_1 (dashed lines refer to the left axis), and thermooptical parameter $\Delta T_0/E_0$ (dotted lines refer to the right axis) for $t_P = 1 \cdot 10^{-8}$ (1),$1 \cdot 10^{-12}$ (2) s for NPs - Au, $\lambda = 532$ nm (a), Ag, $\lambda = 400$ nm (b), Pt, $\lambda = 500$ nm (c), Cu, $\lambda = 570$ nm (d), Pd, $\lambda = 470$ nm (e), Ti, $\lambda = 500$ nm (f), Ni, $\lambda = 470$ nm (g), and Zn, $\lambda = 350$ nm (h) on r_0.

surrounding medium during radiation pulse action for pulse duration $t_P = 1 \times 10^{-8}$ s and bigger ones.

Th maximum value of $(\Delta T_0/E_0)_{max}$ for Au NPs, placed in silica, is equal to $(\Delta T_0/E_0)_{max} = 5.53 \times 10^5$ Kcm^2/J for $r_0 =$ 10 nm, $\lambda = 532$ nm, and $t_P = 1 \times 10^{-12}$ s. Maximum values for Ag NPs, placed in different media, of about $(\Delta T_0/E_0)_{max} \sim (2 - 5) \times 10^6$ Kcm^2/J are achieved with $r_0 = 10$ nm and $t_P = 1 \times 10^{-12}$ s among other NPs. For example, Ag NPs with $r_0 = 10$ nm, placed in water, can achieve the heating of $\Delta T_0 = 100$ K under action of laser pulse with $\lambda = 382$ nm,

$t_P = 1 \times 10^{-10}$, 1×10^{-12} s, and $E_0 = 5.6 \times 10^{-5}$ J/cm^2. It is connected with the achievement of maximum values of K_{abs} for Ag NPs in comparison with other presented NPs.

Figures 4–6 present efficie y factors of absorption K_{abs}, scattering K_{sca}, and extinction K_{ext} for radiation with wavelengths λ in the spectral interval 200–1000 nm for homogeneous metallic spherical NPs with radii 10, 25, and 50 nm, placed in water, for nine different metals.

Figure 4 presents factors of K_{abs}, K_{sca}, and K_{ext} of radiation with wavelengths in the range 300–1000 nm by metallic Pd, Mo, and Cu NPs with radii $r_0 = 10$, 25, and 50 nm placed in water.

Th spectral dependences of K_{abs} and K_{ext} for Cu NPs are smooth enough for $r_0 = 10$ and 25 nm. An interesting feature of these dependences of K_{abs} and K_{ext} on λ for $r_0 = 10$ and 25 nm is the formation of so called "step" (weak dependence of K_{abs} and K_{ext} on λ) for the spectral interval of $\lambda \approx$ 300–565 nm. The e is one weakly defin d maximum in these curves for 310 nm ($r_0 = 10$ nm) and for 387 nm ($r_0 = 25$ nm). We see sharp folding of the dependences of K_{abs} and K_{ext} on λ for $r_0 = 10$ and 25 nm at $\lambda \approx 565$ nm. For $r_0 = 10$ and 25 nm values of $K_{abs} \gg K_{sca}$ and dependences of K_{ext} and K_{abs} on λ are close to each other. The factor of scattering K_{sca} monotonously decreases with increasing λ for $r_0 = 10$ and 25 nm.

In the case of $r_0 = 50$ nm spectral dependences of K_{abs}, K_{sca}, and K_{ext} for Cu NPs have one distinct pronounced maximum: $K_{abs}^{max} \approx 2.7$ for $\lambda_{abs}^{max} = 563$ nm and $K_{sca}^{max} \approx 3.5$, $\lambda_{sca}^{max} = 590$ nm and $K_{ext}^{max} \approx 6$ for $\lambda_{ext}^{max} = 590$ nm. Positions of K_{abs}^{max}, K_{sca}^{max}, and K_{ext}^{max} have been separated in Figure 4 for $r_0 = 50$ nm.

Factor $K_{abs} > K_{sca}$ and $P_1 > 1$ for $r_0 = 10$ and 25 nm and for all presented intervals of wavelengths. But for spectral interval $\lambda \approx$ 570–1000 nm, the value of P_1 is smaller than 1, $P_1 < 1$.

Maximum of K_{abs}^{max} for Pd NP is shift d from the position $\lambda_{abs}^{max} = 230$ nm at $r_0 = 10$ nm to bigger values of λ with increasing r_0 up to $\lambda_{abs}^{max} = 310$ nm and with formation of two weakly defin d maxima of K_{abs}^{max} at $\lambda_{abs}^{max} = 292$ nm and $\lambda_{abs}^{max} = 470$ nm for $r_0 = 50$ nm. The maximum of K_{sca}^{max} is shift d from the values of $\lambda_{sca}^{max} = 190$ nm for $r_0 = 10$ nm to $\lambda_{sca}^{max} = 230$ nm for $r_0 = 25$ nm, and $\lambda_{sca}^{max} = 435$ nm at $r_0 = 50$ nm. The maximum of K_{ext}^{max} is shift d from the values of $\lambda_{ext}^{max} = 190$ nm for $r_0 = 10$ nm to $\lambda_{ext}^{max} = 450$ nm at $r_0 = 50$ nm. We see that the values of K_{abs}^{max}, K_{sca}^{max}, and K_{ext}^{max} have been placed at different positions on λ axis. Parameter P_1 increases up to values of $P_1 \sim$ 10–100 for $r_0 = 10$, 25, and 50 nm with increasing of λ in the range of $\lambda \sim$ 200–1000 nm. For the spectral interval of $\lambda \sim$ 200–600 nm parameter P_1 is smaller than 1, $P_1 < 1$.

Two maximum values of $(\Delta T_0/E_0)_{max}$ are realized in Figures 4(c) and 4(g), for Cu and Pd NPs because two maxima of K_{abs}^{max} have been formed for $r_0 = 50$ nm.

For Mo NPs (Figures 4(e), 4(f), 4(g), and 4(h)) maxima of K_{abs}^{max} are realized in the spectral region 180 ÷ 200 nm for $r_0 = 10$ and 25 nm. Positions of maxima of K_{sca}^{max} and K_{ext}^{max} are shift d from ~200 for $r_0 = 10$ nm to ~230 nm when increasing NP radius up to 25 nm. When the radius is increased up to 50 nm, two maxima of K_{abs}^{max}, K_{sca}^{max}, and K_{ext}^{max} are formed in all curves in Figure 4 (g). Th y are localized in the case of K_{abs}^{max} at $\lambda_{abs}^{max} = 200$ nm and 440 nm, K_{sca}^{max} at $\lambda_{sca}^{max} = 230$ and 420 nm, and K_{ext}^{max} at $\lambda_{ext}^{max} = 210$ and 420 nm. Maximum value of absorption of Mo NPs attains $K_{abs}^{max} \approx 3.2$ for $r_0 = 10$ nm and maximum values scattering and extinction attain $K_{sca}^{max} \approx 2.73$ and $K_{ext}^{max} \approx 4.5$ accordingly for $r_0 = 50$ nm. Two maximum values of $(\Delta T_0/E_0)_{max}$ are realized in Figure 5(g) for Mo NPs.

Figure 5 presents spectral dependences of efficie y factors of K_{abs}, K_{sca}, and K_{ext} of radiation in the range 150–1000 nm by metallic Ni, V, and Ti NPs with radii $r_0 = 10$, 25, and 50 nm, placed in water. Spectral dependences of efficiency factors of K_{abs}, K_{sca}, and K_{ext} for Ni, V, and Ti NPs for radii $r_0 = 10$ nm and 25 nm are smooth curves with maxima in the UV region. With increasing wavelength till 1000 nm absorption, scattering, and extinction slowly decrease. In the case of $r_0 = 50$ nm spectral dependences of efficie y factors of K_{abs} and K_{sca} for V NPs have some weakly defin d maxima located both in UV and in visible region of spectra.

For Ni, V, and Ti NPs we see general features that were early noted for Figures 1–5. The first feature is the shifting of the values of K_{abs}^{max}, K_{sca}^{max}, and K_{ext}^{max} to bigger values of λ with increasing the NP radius; the second one is the shift ng between K_{abs}^{max}, K_{sca}^{max}, and K_{ext}^{max} themselves that means that values of λ_{abs}^{max}, λ_{sca}^{max}, and λ_{ext}^{max} have different values, for example, for Ti NPs with $r_0 = 50$ nm, $\lambda_{abs}^{max} = 505$ nm, $\lambda_{sca}^{max} = 355$ nm, and $\lambda_{ext}^{max} = 450$ nm. The third feature is the formation of second maximums of K_{abs}^{max}; for example, second maximum is formed at $\lambda \approx 480$ nm.

Parameters P_1 for Ni, V, and Ti NPs and for the radiation spectral interval $\lambda \approx$ 150–1000 nm are bigger than 1, $P_1 > 1$, instead of narrow interval $\lambda \approx$ 200–480 nm for V NPs with $r_0 = 50$ nm. Moreover, for $r_0 = 10$ and 25 nm parameters P_1 achieve the values of $P_1 \approx$ 10–500 with increasing λ. It means that Ni, Ti, and V NPs are good absorbers of radiation in wide range of ultraviolet, visible, and infrared optical spectrum.

Figure 6 presents the spectral dependences of K_{abs}, K_{sca}, and K_{ext} for metallic **Co**, **Zn,** and **Al** NPs with radii $r_0 = 10$, 25, and 50 nm, when placed in water. Spectral dependences of efficie y factors of K_{abs}, K_{sca}, and K_{ext} for Co nanoparticles are smooth and have some weakly defin d maxima located both in UV and in visible region of spectra for $r_0 = 10$ and 25 nm. In the case of $r_0 = 50$ nm maximum of absorption is in the UV region of spectra and maxima of scattering and extinction are in the visible one. Th maximum value of absorption for Co NPs is $K_{abs}^{max} \approx 2.5$ for $r_0 = 25$ nm, $\lambda_{abs}^{max} \approx 300$ nm, and maximum values of scattering and extinction are $K_{sca}^{max} \approx 2.2$ and $K_{ext}^{max} \approx 3.9$ for $r_0 = 50$ nm, $\lambda_{sca}^{max} = \lambda_{ext}^{max} = 450$ nm.

For Zn NPs, maxima of spectral dependences of efficie y factors of K_{abs}, K_{sca}, and K_{ext} are sharply defin d, more than for Co NPs, and are shifted in the direction of greater wavelengths. For example, the maximum value of absorption for Zn NPs is $K_{abs}^{max} \approx 4.5$ for $r_0 = 10$ nm, $\lambda_{abs}^{max} \approx 305$ nm, and maximum values of scattering and extinction are $K_{sca}^{max} \approx 4.3$ and $K_{ext}^{max} \approx 5.7$ for $r_0 = 50$ nm, $\lambda_{sca}^{max} \approx 465$ nm. We note the shifti g of K_{sca}^{max} and K_{ext}^{max} to bigger values of λ in comparison with position K_{abs}^{max} for Co and Zn NPs.

Th spectral dependences of efficie y factors of K_{abs}, K_{sca}, and K_{ext} for Al NPs show strongly defin d maxima located mainly in UV. Maximum values of absorption and scattering are close for $r_0 = 10$ nm, and then for $r_0 = 25$ and 50 nm maximum values of scattering are essentially higher than absorption. For example, maximum value of absorption for Al NPs is $K_{abs}^{max} \approx 7.5$ for $r_0 = 10$ nm, $\lambda_{abs}^{max} \approx 190$ nm, and maximum values of scattering and extinction are $K_{sca}^{max} \approx 6$, $K_{ext}^{max} \approx 7$ for $r_0 = 25$ nm, and $\lambda_{sca}^{max} \approx 250$ nm. Factors of K_{sca} and K_{ext} rise to maximum values in the spectral interval 190–500 nm, before decreasing with increasing wavelength in the range 200–1000 nm. Some oscillation structures of the dependences of K_{abs} on λ are formed for Al and Zn NPs with increasing of r_0. It is interesting to note for Al NPs the shift ng of K_{sca}^{max} and K_{ext}^{max} to bigger values of λ and the formation of two maximums of K_{sca}^{max} and K_{ext}^{max} with simultaneous formation of oscillation structure of the K_{abs} dependence on λ with increasing of r_0 to $r_0 = 50$ nm.

Zn NPs with $r_0 = 25$ nm are good absorbers and bad scatterers for all spectral interval of $\lambda \approx 200$–1000 nm. The parameter P_1 for Al NPs is smaller than one ($P_1 < 1$) for $r_0 = 25$ nm in the range of $\lambda \approx 200$–500 nm and for $r_0 = 50$ nm, $\lambda \approx 150$–1000 nm.

Figures 1–6 present spectral dependences of the parameter $\Delta T_0/E_0$ (3) for pulse duration $t_P = 1 \cdot 10^{-8}$, $1 \cdot 10^{-12}$ s for NPs with radii $r_0 = 10$, 25, and 50 nm placed in water. Th range of pulse duration $t_P = 1 \cdot 10^{-8}$–$1 \cdot 10^{-12}$ s is of great interest for laser applications in nanotechnology. Th dependences of parameter $\Delta T_0/E_0$ (3) on λ are analogous to the dependences $K_{abs}(\lambda)$ because of (2a) and (2b). For $\lambda_{abs}^{max} \approx 190$ nm and $r_0 = 10$ nm maximum value of thermooptical parameter for Al NPs achieves value $(\Delta T_0/E_0)_{max} \approx 1.5 \times 10^6$ Kcm^2/J.

Figure 7 presents the dependences of K_{abs}, parameter P_1, and thermooptical parameter $\Delta T_0/E_0$ for $t_P = 1 \cdot 10^{-8}$, $1 \cdot 10^{-12}$ s for metallic NPs, placed in water, and fixed values of λ, for Au NPs, $\lambda = 532$ nm; Ag NPs, $\lambda = 400$ nm; Pt NPs, $\lambda = 500$ nm; Cu NPs, $\lambda = 570$ nm; Ti NPs, $\lambda = 500$ nm; Pd NPs, $\lambda = 470$ nm; Ni NPs, $\lambda = 470$ nm; and Zn NPs, $\lambda = 350$ nm on r_0 in the range of radii $r_0 = 5$–100 nm. The locations of maximum values of $K_{abs}^{max}(r_0)$ and $(\Delta T_0/E_0)_{max}$ (t_P, r_0) are denoted by vertical lines (solid and dotted accordingly). The choice of mentioned wavelengths is determined by their location nearby plasmon wavelengths for these NPs (see Figures 1–6). We consider the results for Au and Ag NPs more closely.

Results for Au NPs are presented in Figure 7(a). The maximum value of $K_{abs}^{max}(r_0, \lambda)$ was calculated and was equal to the next value of r_0: $K_{abs}^{max}(\lambda = 532\,\text{nm}) \approx 3.97$ for $r_0 = 33$ nm. The maximum values of $(\Delta T_0/E_0)_{max}$ for $\lambda = 532$ nm are approximately equal to $(\Delta T_0/E_0)_{max} \approx 4.1 \times 10^5$ Kcm^2/J at $r_0 \approx 23$ nm for $t_P = 1 \cdot 10^{-12}$ s and $(\Delta T_0/E_0)_{max} \approx 6 \times 10^4$ Kcm^2/J at $r_0 \approx 39$ nm for $t_P = 1 \cdot 10^{-8}$ s (see Figure 7(a)). Th maximum values of $K_{abs}^{max}(r_0)$ and $(\Delta T_0/E_0)_{max}$ (r_0) have different locations on r_0 axis for $\lambda = 532$ nm in Figure 7(a). Th maximum values of $(\Delta T_0/E_0)_{max}$ have been shift d by the value $\Delta r_0 \approx 10$ nm to smaller values of r_0 for $t_P = 1 \cdot 10^{-12}$ s and to bigger values of r_0 by the value $\Delta r_0 \approx 6$ nm for $t_P = 1 \cdot 10^{-8}$ s in comparison with the location of K_{abs}^{max} (r_0) in Figure 7(a).

Th maximum values of $(\Delta T_0/E_0)_{max}$ for $\lambda = 532$ nm are achieved for $K_{abs} \approx 3.3$, $t_P = 1 \cdot 10^{-12}$ s, and $r_0 \approx 23$ nm and for $K_{abs} \approx 3.6$, $t_P = 1 \cdot 10^{-8}$ s, and $r_0 \approx 39$ nm. It means that for achievement of the maximum values of $(\Delta T_0/E_0)_{max}$ under minimal values of E_0 we have to use the values of K_{abs} that are smaller than K_{abs}^{max} mentioned above.

Th differences between the values of $\Delta T_0/E_0$ for $t_P = 1 \cdot 10^{-8}$ s and $t_P = 1 \cdot 10^{-12}$ s decrease with increasing r_0. These differences are about ~10^2-10^3 times for $r_0 = 10$ nm and are equal to only ~2-3 times for $r_0 = 100$ nm. It can be explained by a sharp increase of $\tau_T \sim r_0^2$ and approaching of τ_0 to $t_P = 1 \cdot 10^{-8}$ s for $r_0 \geq 90$–100 nm and fulfillment of short pulse condition (without heat loss).

Th characteristic time τ_T is equal to $\tau_T \sim 1.2 \cdot 10^{-10}$–$3.2 \cdot 10^{-9}$ s for the range $r_0 = 10$–50 nm and for ambient water $k_\infty = 6 \cdot 10^{-3}$ W/cmK, $\tau_T \sim 0.9$ ns for $r_0 = 25$ nm. The fulfillment of the condition $t_P < \tau_T$ (1) for the most interesting range of r_0 : $25 < r_0 < 50$ nm means that the value of t_P will be in the range of pulse durations: $t_P < 1 \cdot 10^{-9}$ s.

Th condition of "short" pulses $t_P < \tau_T$ is applicable for $t_P = 1 \cdot 10^{-12}$ s for all values of r_0 : $5 < r_0 < 100$ nm. Under condition of "short" pulses $t_P < \tau_T$, the parameter $\Delta T_0/E_0$ depends on the combination K_{abs}/r_0 and, accordingly, equation (3) describing the increasing and decreasing of $\Delta T_0/E_0$.

Th condition of "long" pulses with $t_P = 1 \cdot 10^{-8}$ s is also fulfil ed for the interval $r_0 = 5$–100 nm. The use of "long" pulses with $t_P = 1 \cdot 10^{-8}$ s leads to a significant decrease of the value of $\Delta T_0/E_0$ up to 1-2 orders and more in comparison with cases for $t_P = 1 \cdot 10^{-12}$ s for the whole range of $r_0 = 5$–100 nm. It is determined by heat conduction losses from NP during irradiation with this value of t_P and because of the dependence $\Delta T_0/E_0 \sim 1/t_P$ (see (3)).

From (4a) and (4b) we see that

$$t_P < \tau_T, \quad \frac{\Delta T_0}{E_0} \sim \frac{K_{abs}(r_0)}{r_0}, \qquad t_P > \tau_T, \quad \frac{\Delta T_0}{E_0} \sim K_{abs}(r_0)\, r_0. \tag{5}$$

Our results are in accordance with presented dependences (5).

Figure 7(b) presents the dependences of parameter $\Delta T_0/E_0$ (r_0, λ) (3) and K_{abs} (r_0, λ) for Ag NPs and for the pulse durations $t_P = 1 \cdot 10^{-8}$, $1 \cdot 10^{-12}$ s, and $\lambda = 400$ nm on r_0. Maximum values of $(\Delta T_0/E_0)_{max}$ for Ag NPs are equal to $\approx 1.1 \times 10^6$ Kcm^2/J, $t_P = 1 \cdot 10^{-12}$ s, and $r_0 \sim 19$nm and $\approx 5.1 \times 10^4$ Kcm^2/J, and $t_P = 1 \cdot 10^{-8}$ s at $r_0 \sim 21$nm in the range 5–100 nm (see Figure 7(b)). Heating of NP with $r_0 \sim 19$nm and for $t_P \leq 1 \cdot 10^{-10}$ s could achieve $1 \cdot 10^3$ K under radiation energy density $E_0 = 1 \times 10^{-3}$ J/cm^2.

The e are three maximums of K_{abs}^{max} and correspondingly three maximum values of $(\Delta T_0/E_0)_{max}$ for $t_P = 1 \times 10^{-12}$ s, placed at $r_0 \approx 19$, 58, and 95 nm, in the range of $r_0 = 5$–100 nm. Oscillated dependences of $\Delta T_0/E_0$ behave in an

analogous manner to the dependences of K_{abs} on r_0 for the presented values of λ (see Figure 7(b)). Values of $\Delta T_0/E_0$ for $t_P = 1\times10^{-8}$ s are smaller than the ones for $t_P = 1\times10^{-12}$ s for the whole range of r_0 = 5–100 nm. The values of shift between the locations of K_{abs}^{max} and $(\Delta T_0/E_0)_{max}$ for Ag NPs are smaller than in the case of Au NPs because of sharp dependences of K_{abs} on r_0, especially for λ = 400 nm (see Figure 7(b)).

The dependences of K_{abs}, P_1, and $\Delta T_0/E_0$ on r_0 for fixed values of λ for Pt, Cu, Pd, Ti, and Ni NPs are generally analogous to the dependences of Au NPs. The dependences of Zn NP parameters on r_0 are analogous to the dependences of Ag NPs. For all metallic NPs maximum values of $(\Delta T_0/E_0)_{max}$ are shifted compared to location K_{abs}^{max} in Figure 7(b) to smaller values of r_0 for "short" pulses $t_P < \tau_T$ and to bigger values of r_0 for "long" pulses $t_P > \tau_T$.

Figures 1–6 present the dependences of P_1 on λ for metallic NPs with radii r_0 = 10, 25, and 50 nm and metals Ag, Al, Au, Co, Cu, Mo, Ni, Pd, Pt, Ti, V, and Zn. Dependences of P_1 on λ are determined by the correlation between dependences of $K_{abs}(\lambda)$ and $K_{sca}(\lambda)$. Dependences of P_1 on λ for different values of r_0 have complicated disposition. For NPs with r_0 = 10 nm all presented metallic NPs exhibit high absorbance and parameter $P_1 \gg 1$ for all metallic NPs and in part $P_1 > 1$ for some spectral intervals. The maximum values reached $P_1 \geq 100$ for Co, Mo, Ni, Pd, Pt, Ti, V, and Zn NPs for interval $600 > \lambda > 1000$ nm and for Au and Cu NPs maximum $P_1 \sim 100$ for $300 > \lambda > 500$ nm for r_0 = 10 nm. All mentioned NPs are the best absorbers with $P_1 \geq 10 \div 100$ for $600 > \lambda > 1000$ nm and r_0 = 10 and 25 nm instead of Au and Cu NPs. Increasing of r_0 leads to an increase in scattering and decrease in absorbance for all presented metallic NPs. Therefore, larger NPs are more suitable for light-scattering based applications. At r_0 = 50 nm instead of spectral interval $600 < \lambda < 1000$ nm for Co, Mo, Ni, Pd, Ti, and Zn NPs all values of P_1 are smaller or much smaller than 1, $P_1 \ll 1$. Best scattering NPs among the studied metallic NPs are Ag NPs for $r_0 > 20$ nm. It is interesting to note that NPs can be used as absorbers in one interval of wavelengths and as scatterers in different intervals of wavelengths. All NPs with r_0 = 25 nm could be the scatterers in the interval $300 < \lambda < 500$ nm and the absorbers in the interval $500 < \lambda < 1100$ nm. Variant with value $P_1 \approx 1$ means approximately equal possibility of using NP as absorber and scatterer simultaneously.

A predominant role of absorption by NP can be used for heating of NP for thermoplasmonic applications. Such NPs can be used as absorbers of radiation. A predominant role of scattering by NPs can be used for the purposes of optical diagnostics and imaging using scattered radiation. The selection of ratio between scattering and absorption with $P_1 < 1$ provides a tool for NP for contrast applications in scattering optical diagnostics.

4. Conclusions

The strongly enhanced absorption and scattering of spherical metallic NPs make them a novel and highly effective class of contrast agents for photothermal applications and imaging-based optical diagnostics. A number of factors need to be optimized for the success in these fields. These ones include the efficiency factors of absorption K_{abs}, scattering K_{sca}, and extinction K_{ext} of radiation by NP, parameters of P_1, and $\Delta T_0/E_0$. There is a need to study the dependence of these parameters on the type of metal and size of NP, radiation wavelength, parameters of surrounding medium, and so forth. Systematic study of all these characteristics is a prerequisite for the successful transition of the research promise of metallic NPs to thermal applications and has been carried out in this paper.

We conducted the investigation and analysis of plasmonic (K_{abs}, K_{sca}, and K_{ext}) and thermooptical ($\Delta T_0/E_0$) characteristics of 12 metallic NPs for radiation wavelengths in the spectral interval 200–1000 nm and in the range of NP radii r_0 = 5–100 nm, especially for r_0 = 10, 25, and 50 nm, based on computer and analytical modeling (Figures 1–7). Different metals were used for NPs, Au, Ag, Cu, Pt, Co, Zn, Al, Ni, Ti, V, Pd, and Mo. Three surrounding NP media were used, silica, water, and air. Value of refractive index of surroundings in the range $n_\lambda = 1.51 - 1.0$ influences the plasmonic properties with the change. The use of silica as surroundings leads to rather small deviations from the dependences with water as ambience. More pronounced deviations of NP optical and thermooptical characteristics have been determined for air surrounding.

The selection of different NPs is based on the investigation of the influence of different parameters of NP itself, radiation pulses, and ambient medium on NP properties.

The data in Figures 1–7 allow estimating the possibility to use different metallic NPs for thermoplasmonics and photonic applications. Maximum values of K_{abs} were achieved for Au, Ag, Zn, and Cu. Transformation of plasmonic (K_{abs}, K_{sca}, and K_{ext}) and thermooptical ($\Delta T_0/E_0$) properties in dependence on λ, r_0 with changing of NP, radiation, and ambience parameters is presented in Figures 1–7. Positions λ_{abs}^{max}, λ_{sca}^{max}, and λ_{ext}^{max} of maximum values of K_{abs}^{max}, K_{sca}^{max}, and K_{ext}^{max} have been determined on λ axis and in some cases the positions of K_{abs}^{max}, K_{sca}^{max}, and K_{ext}^{max} do not coincide.

Parameter of P_1 can be used for determination of the use of NP predominantly as an absorber for $P_1 > 1$ or as a scatterer for $P_1 < 1$. It is interesting to note the achievement of values of $P_1 \geq 10$–100 for mentioned NPs with r_0 = 10 and 25 nm instead of Ag and Al NPs in some spectral intervals. Larger NPs are more suitable for light-scattering based applications. Best scattering NPs inside presented metallic NPs are Ag NPs for $r_0 > 20$ nm. It is interesting to note Al NPs with r_0 = 25 nm which can be used as absorbers in one wavelength interval ($1100 > \lambda > 500$ nm) and as scatterers in the different one ($500 > \lambda > 300$ nm).

The main goal of light-to-thermal energy conversion and thermoplasmonics is to achieve maximum value of efficiency parameter of $\Delta T_0/E_0$ for NPs at minimal values of E_0. The influence of the parameters of radiation, t_P, λ, and E_0 of NP, ρ_0, c_0, r_0, K_{abs}, and surrounding medium, k_∞ and n_λ, reach a maximum value of $\Delta T_0/E_0$ has been established based on an analytical model. It is possible to achieve the values of about $\Delta T_0/E_0 \sim 1\cdot10^6$ Kcm^2/J for NPs and for $t_P \leq 1\cdot10^{-10}$ s under radiation energy density $E_0 = 1\cdot10^{-3}$ J/cm^2 and the heating of such NP could achieve $1\cdot10^3$ K.

Th selection of appropriate properties of NPs is based on the choice of value of r_0 for the values of determined λ and t_P and the choice of metallic NPs, λ, and t_P for the determined value of r_0.

It was established that maximum values of $\Delta T_0/E_0$ and of NP temperature can be achieved with the use of the value of absorption efficiency factor K_{abs} smaller than maximum value of $K_{\text{abs}}^{\max}$ taking into account irradiation duration, characteristics of NPs, and their cooling. Shif t f the positions of maximum value of $\Delta T_0/E_0$ from the location of maximum value of $K_{\text{abs}}^{\max}$ on axis r_0 is determined by noticeable influence of r_0 on the processes of NP heating and cooling.

Our results allow estimating of optimal characteristics of absorption and scattering radiation by NPs and laser energy conversion into photothermal phenomena by selection of the NP and radiation parameters and ambience properties. We present a platform for selection of the plasmonic and thermooptical properties of metallic NPs, placed in different media, for their photonic and thermoplasmonic applications.

Conflict of Interests

The authors declare that there is no conflict of interests regarding the publication of this paper.

References

[1] J. R. Adleman, D. A. Boyd, D. G. Goodwin, and D. Psaltis, "Heterogenous catalysis mediated by plasmon heating," *Nano Letters*, vol. 9, no. 12, pp. 4417–4423, 2009.

[2] R. Narayanan and M. A. El-Sayed, "Some aspects of colloidal nanoparticle stability, catalytic activity, and recycling potential," *Topics in Catalysis*, vol. 47, no. 1-2, pp. 15–21, 2008.

[3] N. J. Halas, "Th photonic nanomedicine revolution: let the human side of nanotechnology emerge," *Nanomedicine*, vol. 4, no. 4, pp. 369–371, 2009.

[4] L. C. Kennedy, L. R. Bickford, N. A. Lewinski et al., "A new era for cancer treatment: gold-nanoparticle-mediated thermal therapies," *Small*, vol. 7, no. 2, pp. 169–183, 2011.

[5] X. Huang, P. K. Jain, I. H. El-Sayed, and M. A. El-Sayed, "Plasmonic photothermal therapy (PPTT) using gold nanoparticles," *Lasers in Medical Science*, vol. 23, no. 3, pp. 217–228, 2008.

[6] V. K. Pustovalov, A. S. Smetannikov, and V. P. Zharov, "Photothermal and accompanied phenomena of selective nanophotothermolysis with gold nanoparticles and laser pulses," *Laser Physics Letters*, vol. 5, no. 11, pp. 775–792, 2008.

[7] V. Pustovalov, L. Astafyeva, and B. Jean, "Computer modeling of the optical properties and heating of spherical gold and silica-gold nanoparticles for laser combined imaging and photothermal treatment," *Nanotechnology*, vol. 20, no. 22, Article ID 225105, 2009.

[8] V. Pustovalov, L. Astafyeva, E. Galanzha, and V. Zharov, "Thermo-optical analysis and selection of the properties of absorbing nanoparticles for laser applications in cancer nanotechnology," *Cancer Nanotechnology*, vol. 1, pp. 35–46, 2010.

[9] A. Csaki, F. Garwe, A. Steinbrück et al., "A parallel approach for subwavelength molecular surgery using gene-specifi positioned metal nanoparticles as laser light antennas," *Nano Letters*, vol. 7, no. 2, pp. 247–253, 2007.

[10] J. Wang, J. D. Byrne, M. E. Napier, and J. M. Desimone, "More effective nanomedicines through particle design," *Small*, vol. 7, no. 14, pp. 1919–1931, 2011.

[11] S. Jain, D. Hirst, and J. O'Sullivan, "Gold nanoparticles as novel agents for cancer therapy," *British Journal of Radiology*, vol. 85, no. 1010, pp. 101–113, 2012.

[12] N. Zheludev, "Single nanoparticle as photonic switch and optical memory element," *Journal of Optics A: Pure and Applied Optics*, vol. 8, no. 4, pp. S1–S9, 2006.

[13] M. Pelton, J. Aizpurua, and G. Bryant, "Metal-nanoparticle plasmonics," *Laser and Photonics Reviews*, vol. 2, no. 3, pp. 136–159, 2008.

[14] Y. Sonnefraud, A. L. Leen Koh, D. W. McComb, and S. A. Maier, "Nanoplasmonics: engineering and observation of localized plasmon modes," *Laser and Photonics Reviews*, vol. 6, no. 3, pp. 277–295, 2012.

[15] Y. Jin, Q. Li, G. Li et al., "Enhanced optical output power of blue light-emitting diodes with quasi-aligned gold nanoparticles," *Nanoscale Research Letters*, vol. 9, no. 1, pp. 7–13, 2014.

[16] S. Inasawa, M. Sugiyama, S. Noda, and Y. Yamaguchi, "Spectroscopic study of laser-induced phase transition of gold nanoparticles on nanosecond time scales and longer," *Journal of Physical Chemistry B*, vol. 110, no. 7, pp. 3114–3119, 2006.

[17] H. Muto, K. Miyajima, and F. Mafuné, "Mechanism of laser-induced size reduction of gold nanoparticles as studied by single and double laser pulse excitation," *Th Journal of Physical Chemistry C*, vol. 112, no. 15, pp. 5810–5815, 2008.

[18] A. Pyatenko, M. Yamaguchi, and M. Suzuki, "Mechanisms of size reduction of colloidal silver and gold nanoparticles irradiated by Nd:YAG laser," *Journal of Physical Chemistry C*, vol. 113, no. 21, pp. 9078–9085, 2009.

[19] S. Hashimoto, D. Werner, and T. Uwada, "Studies on the interaction of pulsed lasers with plasmonic gold nanoparticles toward light manipulation, heat management, and nanofabrication," *Journal of Photochemistry and Photobiology C: Photochemistry Reviews*, vol. 13, no. 1, pp. 28–54, 2012.

[20] J. Wang, Y. Chen, X. Chen, J. Hao, M. Yan, and M. Qiu, "Photothermal reshaping of gold nanoparticles in a plasmonic absorber," *Optics Express*, vol. 19, no. 15, pp. 14726–14734, 2011.

[21] M. Honda, Y. Saito, N. I. Smith, K. Fujita, and S. Kawata, "Nanoscale heating of laser irradiated single gold nanoparticles in liquid," *Optics Express*, vol. 19, no. 13, pp. 12375–12383, 2011.

[22] A. L. Stepanov, "Nonlinear optical properties of implanted metal nanoparticles in various transparent matrixes: a review," *Reviews on Advanced Materials Science*, vol. 27, no. 2, pp. 115–145, 2011.

[23] A. Stalmashonak, G. Seifert, and A. Abdolvand, *Ultra-Short Pulsed Laser Engineered Metal-Glass Nanocomposites*, Springer, New York, NY, USA, 2013.

[24] V. K. Pustovalov, "Th oretical study of heating of spherical nanoparticle in media by short laser pulses," *Chemical Physics*, vol. 308, no. 1-2, pp. 103–109, 2005.

[25] A. O. Govorov and H. H. Richardson, "Generating heat with metal nanoparticles," *Nano Today*, vol. 2, no. 1, pp. 30–38, 2007.

[26] V. K. Pustovalov, L. G. Astafyeva, and W. Fritzsche, "Selection of thermo-optical parameter of nanoparticles for achievement of their maximal thermal energy under optical irradiation," *Nano Energy*, vol. 2, no. 6, pp. 1137–1141, 2013.

[27] G. Baffou and R. Quidant, "Thermo-plasmonics: using metallic nanostructures as nano-sources of heat," *Laser and Photonics Reviews*, vol. 7, no. 2, pp. 171–187, 2013.

[28] U. Kreibig and M. Vollmer, *Optical Properties of Metal Clusters*, vol. 25 of *Springer Series in Material Science*, Springer, Heidelberg, Germany, 1995.

[29] C. F. Bohren and D. R. Huffman, *Absorption and Scattering of Light by Small Particles*, Wiley, New York, NY, USA, 1983.

[30] V. K. Pustovalov and V. A. Babenko, "Optical properties of gold nanoparticles at laser radiation wavelengths for laser applications in nanotechnology and medicine," *Laser Physics Letters*, vol. 1, no. 10, pp. 516–520, 2004.

[31] P. K. Jain, X. Huang, I. H. El-Sayed, and M. A. El-Sayed, "Review of some interesting surface plasmon resonance-enhanced properties of noble metal nanoparticles and their applications to biosystems," *Plasmonics*, vol. 2, no. 3, pp. 107–118, 2007.

[32] M. G. Blaber, M. D. Arnold, and M. J. Ford, "Search for the ideal lasmonic nanoshell: the effects of surface scattering and alternatives to gold and silver," *Journal of Physical Chemistry C*, vol. 113, no. 8, pp. 3041–3045, 2009.

[33] V. Amendola, O. M. Bakr, and F. Stellacci, "A study of the surface plasmon resonance of silver nanoparticles by the discrete dipole approximation method: effect of shape, size, structure, and assembly," *Plasmonics*, vol. 5, no. 1, pp. 85–97, 2010.

[34] S. A. Joseph, S. Mathew, G. Sharma et al., "Photothermal characterization of nanogold under conditions of resonant excitation and energy transfer," *Plasmonics*, vol. 5, no. 1, pp. 63–68, 2010.

[35] P. R. West, S. Ishii, G. V. Naik, N. K. Emani, V. M. Shalaev, and A. Boltasseva, "Searching for better plasmonic materials," *Laser and Photonics Reviews*, vol. 4, no. 6, pp. 795–808, 2010.

[36] Y. Sonnefraud, A. Koh, D. W. McComb, and S. A. Maier, "Nanoplasmonics: engineering and observation of localized plasmon modes," *Laser and Photonics Reviews*, vol. 6, no. 3, pp. 277–295, 2012.

[37] A. Chen and P. Holt-Hindle, "Platinum-based nanostructured materials: synthesis, properties, and applications," *Chemical Reviews*, vol. 110, no. 6, pp. 3767–3804, 2010.

[38] M. B. Cortie and A. M. McDonagh, "Synthesis and optical properties of hybrid and alloy plasmonic nanoparticles," *Chemical Reviews*, vol. 111,no. 6, pp. 3713–3735, 2011.

[39] M. Rycenga, C. M. Cobley, J. Zeng et al., "Controlling the synthesis and assembly of silver nanostructures for plasmonic applications," *Chemical Reviews*, vol. 111,no. 6, pp. 3669–3712, 2011.

[40] P. B. Johnson and R. W. Christy, "Optical constants of the noble metals," *Physical Review B*, vol. 6, no. 12, pp. 4370–4379, 1972.

[41] E. D. Palik, *Handbook of Optical Constants of Solids*, Academic Press, New York, NY, USA, 1998.

[42] SOPRA N & K database [Electronic resource], http://refractiveindex.info/.

[43] E. Grigor'ev and E. Meilikhov, *Physical Quantities*, Atomizdat, Moscow, Russia, 1991.

[44] F. Kreith and W. Z. Black, *Basic Heat Transfer*, Harper and Row, New York, NY, USA, 1980.

[45] N. C. Bigall, T. Härtling, M. Klose, P. Simon, L. M. Eng, and A. Eychmüller, "Monodisperse platinum nanospheres with adjustable diameters from 10 to 100 nm: synthesis and distinct optical properties," *Nano Letters*, vol. 8, no. 12, pp. 4588–4592, 2008.